Structure and magnetism in $LaCoO_3$

D. P. Belanger,[1] T. Keiber,[1] F. Bridges,[1] A. M. Durand,[1] A. Mehta,[2] H. Zheng,[3] J. F. Mitchell,[3] and V. Borzenets[2]

[1]*Department of Physics, University of California, Santa Cruz, CA 95064, USA*
[2]*Stanford Synchrotron Radiation Lightsource, SLAC National Accelerator Laboratory, Menlo Park, California 94025, United States*
[3]*Materials Science Division, Argonne National Laboratory, Argonne, IL 60439, USA*

(Dated: October 26, 2015)

The temperature dependence of the hexagonal lattice parameter c of single crystal $LaCoO_3$ (LCO) with $H = 0$ and 800 Oe, as well as LCO bulk powders with $H = 0$, was measured using high-resolution x-ray scattering near the transition temperature $T_o \approx 35$ K. The change of $c(T)$ is well characterized by a power law in $T - T_o$ for $T > T_o$ and by a temperature independent constant for $T < T_o$ when convoluted with a Gaussian function of width 8.5 K. This behavior is discussed in the context of the unusual magnetic behavior observed in LCO as well as recent generalized gradient approximation calculations.

PACS numbers:

arXiv:1510.07002v1 [cond-mat.str-el] 23 Oct 2015

$LaCoO_3$ (LCO) exhibits magnetic behaviors that cannot be explained using local Co ion spin state transitions alone. Experiments and calculations have shown the importance of extended states [1–4] and rhombohedral distortion near a transition at $T_o \approx 35$ K that involves the Co-O-Co bond angle. A core-interface model was developed [5, 6] that includes strained interface regions near surfaces and interfaces with impurity phases, particularly Co_3O_4, and core regions far from such surfaces and interfaces. In this model, ferromagnetic long-range order below $T_C = 89$ K is associated with the interface regions. This is similar to the case of thin films which have strained interfaces with substrates that generate ferromagnetic moments. [7] For bulk particles and single crystals, most of the spins are in the core regions that are dominated by antiferromagnetic interactions, though the core regions never develop antiferromagnetic or ferromagnetic long-range order.

Neither indirect [8] nor direct [1, 2] experimental observations yielded any evidence of a Jahn-Teller distortion of the oxygen octahedra surrounding Co ions. This eliminated one model proposed [9] that would have accounted for the magnetic behavior or LCO through modification of the local spin excitations, allowing excitations of order 100 K in local-density approximation calculations to explain the magnetic behavior near 100 K. On the other hand, generalized gradient approximation (GGA) calculations [4] show that extended states can account for excitations in the required energy range without the Jahn-Teller distortion of the oxygen octahedra and this is in better agreement with the experimental observations. As the temperature decreases from room temperature, the behavior of the inverse magnetization, H/M vs T, indicates that antiferromagnetic correlations in the core region increase below T_C, reach a broad maximum near $T = 40$ K and then decrease substantially. [5]

It was shown in neutron scattering studies [5, 10] that, as the temperature decreases towards T_o, the Co-O-Co angle γ rapidly approaches an angle $\gamma = 163°$. Below $T \approx 40$ K, little change in the angle was observed. Generalized gradient approximation (GGA) calculations [4] indicate LCO to be non-magnetic for $\delta y = \frac{d}{a}\cos(\gamma/2)$ above a critical value of 0.052, where a is the hexagonal lattice parameter and d is the Co-O bond length. This critical value for δy corresponds to $\gamma_C = 163°$ using the measured low T bulk powder values $a = 5.40$ Å and $d = 1.915$ Å. [10] This agrees with the experimental observations [10] for $T \leq 40$ K.

To further explore the relationship between the structural changes and the magnetic behavior, we have used high resolution x-ray scattering techniques. Although x-ray scattering is less sensitive to the oxygen positions and is usually less reliable to directly measure the Co-O-Co bond angle, it was observed [10] that the transition near To is also expressed in the behavior of all the lattice parameters. Hence, the transition can be studied with high resolution using, for example, x-ray measurements of the temperature dependence of the c hexagonal lattice parameter. We have used high resolution x-ray scattering measurements of c versus T to better characterize the nature of the transition at T_o. In addition, we have explored the dependence of the transition upon application of a small magnetic field in single crystals and we have compared the behavior of single crystals and a bulk LCO powder. From the results of the experimental measurements, we propose a model to understand how LCO develops from the low T non-magnetic state to a magnetic state for $T > 40$ K.

The bulk particles of the powder samples were synthesized using a standard solid state reaction. Bulk Co_3O_4 and La_2O_3 were ground together using a mortar and pestle and then heated to 850°C - 1050°C for approximately 8 hours in air. The grinding and heating processes were repeated five times, with a final 24 hour heating at 1100°C. Neutron powder diffraction characterizations indicate the primary phase is $LaCoO_3$, with a

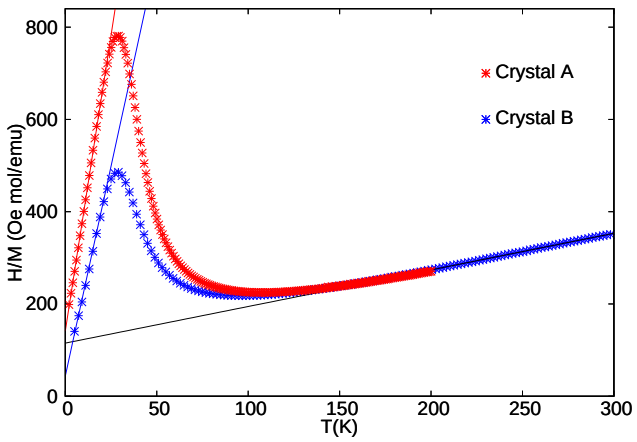

FIG. 1: M/H vs T for two single crystals, A and B (see text), with $H = 1$ T along with Curie-Weiss fits (Eq. 1) for $170 < T < 300$ K and for low temperature.

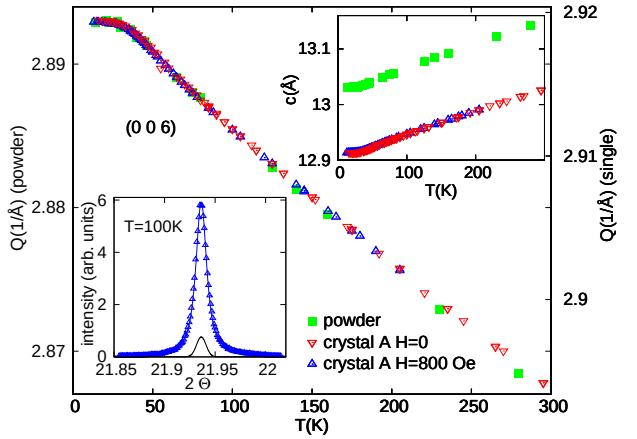

FIG. 2: The temperature dependence of Q for crystal A, for $H = 0$ and $H = 800$ Oe, and the bulk powder for $H = 0$, determined from the (0 0 6) Bragg positions. The upper insert shows the hexagonal c lattice parameters. There is no observed difference between cooling and heating data. The lower insert shows a fit to the very sharp (0 0 6) diffraction peak using a sum of a Lorentzian and a Gaussian; the small Gaussian contribution is below the data and combined fit.

small amount, 4.5(4)% by weight, of the impurity phase Co_3O_4.

To synthesize the two single crystals, labeled A and B, a stoichiometric powder of $LaCoO_3$ was prepared from La_2O_3 (prefired at 1000°C immediately prior to use) and Co_3O_4, pressed into rods, and sintered in air. Single crystals of $LaCoO_3$ were then grown from the rods using an IR optical-image floating zone technique (model NEC SC15-HD) in a 100% O_2/Ar atmosphere. Samples were found to be single phase $LaCoO_3$ by powder x-ray diffraction of a pulverized section of the crystal.

The magnetization of crystals A and B was measured using a Quantum Design 9T Physical Properties Measurement System (PPMS). No attempt was made to

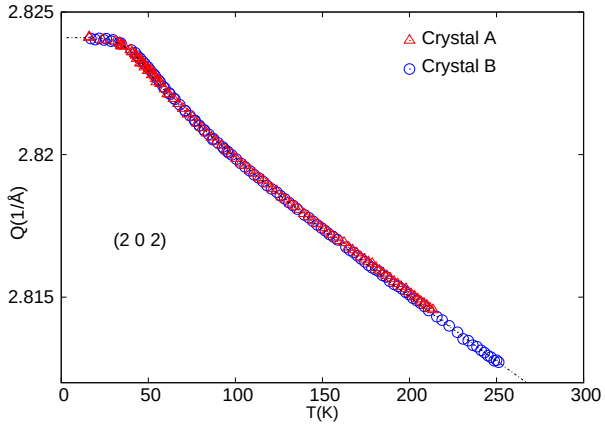

FIG. 3: The temperature dependence of Q for crystals A and B, determined from the (2 0 2) Bragg positions. There is no observed difference between cooling and heating data.

align the crystals for the measurements, as they are heavily twinned. The inverse magnetization, shown for $H = 10$ kOe as H/M vs T in Fig. 1, indicates, from the straight line behavior for $170 < T < 300$, that the single crystals are dominated by antiferromagnetic interactions, consistent with bulk powders measured previously. A fit of the Curie-Weiss behavior,

$$M/H = \frac{C}{T - \theta_{CW}}, \qquad (1)$$

to the data from crystal B for $170 < T < 300$ K yields $C = 1.26 \pm 0.02$ emu·K/mol and $\theta_{CW} = -145 \pm 5$ K, which suggests a slightly weaker antiferromagnetic system than the the bulk powder, which gave $C = 1.49 \pm 0.02$ emu·K/mol and $\theta_{CW} = -182 \pm 4$ K in a previous bulk powder study. [10] The average effective moment is $\mu_{eff} = 3.17(2)\ \mu_B$ per Co ion, using $\mu_{eff}^2/\mu_B^2 = 3k_BC/N_A$, where μ_B is the Bohr magneton, N_A is Avogadro's number, and k_B is the Boltzmann constant. This is smaller than the value $\mu_{eff} = 3.45(2)\ \mu_B$ obtained for a LCO bulk powder. [10] The negative value of θ_{CW} indicates antiferromagnetic interactions and, from its magnitude, the system might be expected to exhibit antiferromagnetic long-range order below $T \approx 100$ K, but that is never observed. Below $T \approx 30$ K, a fit to the Curie-Weiss expression yields $\theta_{CW} = -5.5 \pm 0.5$ K and $C = 0.39 \pm 0.02$ emu·K/mol for Crystal A and $\theta_{CW} = -2.4 \pm 0.5$ K and $C = 0.55 \pm 0.02$ emu·K/mol for Crystal B. The various Curie-Weiss results are summarized in Table I. Unlike the parameters obtained for $T > 170$ K, where the interactions are sufficiently weak, the Curie-Weiss parameters at low T are not directly interpretable in terms of the moment and interaction strength because the short-range correlations are not weak over the range $10 < T < 35$ K. Furthermore, the behavior is field-dependent. [5] Rather, this behavior likely represents a decrease in magnetic long-range correlations and a rapid

TABLE I: Curie-Weiss parameters using Eq. 1 for crystals A and B and the bulk powder, measured with $H = 1$ T.

	A	**B**	**bulk powder**
		170 < T < 300 K	
C (emu·K/mol)	-	1.26(2)	1.49(2)
θ_{CW} (K)	-	-145(5)	-182(4)
μ_{eff} (μ_B)	-	3.17(2)	3.45(2)
		T < 30 K	
C (emu·K/mol)	0.39(2)	0.55(2)	-
θ_{CW} (K)	-5.5(5)	-2.4(5)	-

approach to the $T = 0$ susceptibility. The low T state is more complex than would be predicted in a $S = 0$ local Co spin state model and low temperature models have been proposed. [8, 11] It was shown [5] for bulk particles that the height of the peak in H/M vs T increases with a decrease in the dominant impurity phase Co_3O_4 and, while Co_3O_4 is likely absent in the single crystals, the difference in peak height between crystal A and B is probably a result of the presence of fewer twinning planes and other defects in crystal A. Consistent with the interpretation that crystal A is higher in quality, crystal A exhibits fewer strong scattering peaks from crystal twinning relative to crystal B.

High resolution x-ray data were collected as a function of temperature on beam line 10-2 at SSRL using either 15 or 20 keV photons. The twinned single crystal samples were mounted on a thick copper block, with the (111) axis of the pseudo-cubic cell vertical; all reflections were in a vertical plane. For twinned crystals the (006) hexagonal (c axis) reflection and the (202) from another twin are close in angle, but were easily resolved. A Sunpower Stirling cryocooler (CryTel-MT) cryostat was used with a calibrated thermometer mounted on the copper block close to the sample. Each time the temperature was changed, it took 10-12 minutes for equilibrium to be established such that no hysteresis was observed. At each temperature, the full line shape was recorded, (e.g. inset of Fig. 2). For the measurements in the applied field, permanent magnets were mounted close to the sample on opposing sides.

We studied the temperature behavior of the c lattice parameter of LCO, using the $R\bar{3}c$ crystal structure, by examining the hexagonal lattice (0 0 6) Bragg peak as a function of temperature for crystal A and the bulk powder, as shown in Fig. 2. For the crystal, we took measurements in zero field and in a field $H = 800$ Oe. This field strength is known to be sufficient to suppress much of the ferromagnetic ordering in bulk powders [5]. However, no difference is discernible between the data with 800 Oe applied perpendicularly to the c axis and data taken in zero field. We also observed no difference between cooling and heating. Powder data are also shown in Fig. 2 and have nearly the same temperature dependence as the single crystal, but with a slightly smaller overall value for

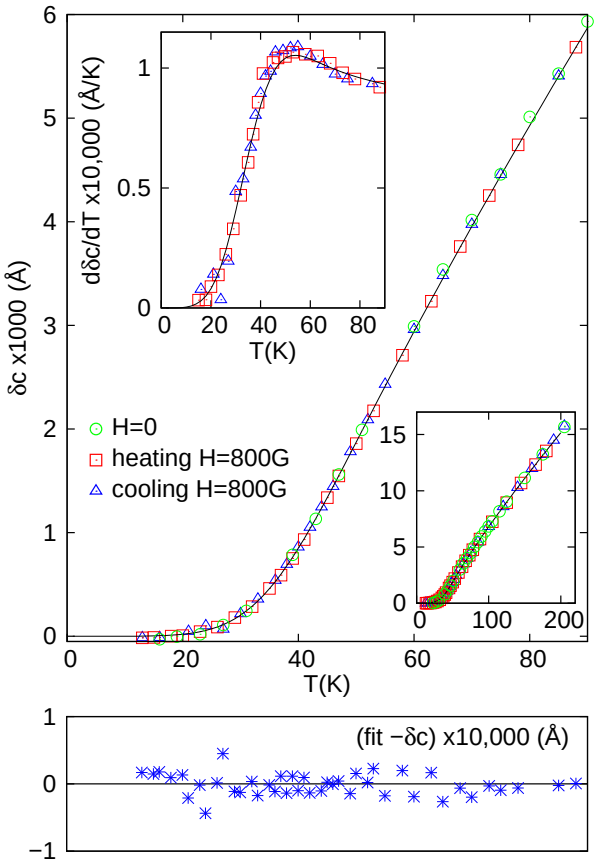

FIG. 4: The change in the c lattice parameter with temperature with a fit to Eq. 2 shown by the solid curve, for crystal A with $H = 0$ (circle) and 800 G (squares/triangles). There is no significant difference between the cooling and heating data. The upper insert shows the derivative of the change in c vs T (same point symbols) and the derivative of the fit shown in the main figure for $H = 800$ G. The lower insert is the same as the main figure, but extending to higher temperature. The bottom panel shows the fit minus the data (times 10^4) for the $H = 800$ G data shown in the main figure.

Q, the magnitude of the scattering vector. The inset of Fig. 2 shows the lattice parameter $c = 12\pi/Q$ vs T; the c parameter for the powder is larger than that of the single crystal.

For crystals A and B in zero field, Q vs T at the (2 0 2) Bragg peak is shown in Fig. 3. No significant difference between the two crystals is discernible and there is no observed difference between data taken upon cooling and heating. It is not straightforward to interpret the shape of the curves for this Bragg point because it involves both the a and c lattice parameters.

We find that we can obtain an excellent fit to the $H = 0$ and 800 Oe c vs T data from crystal A using a power law in $T - T_o$ for $T > T_o$ and no change for $T < T_o$ convoluted with a Gaussian function,

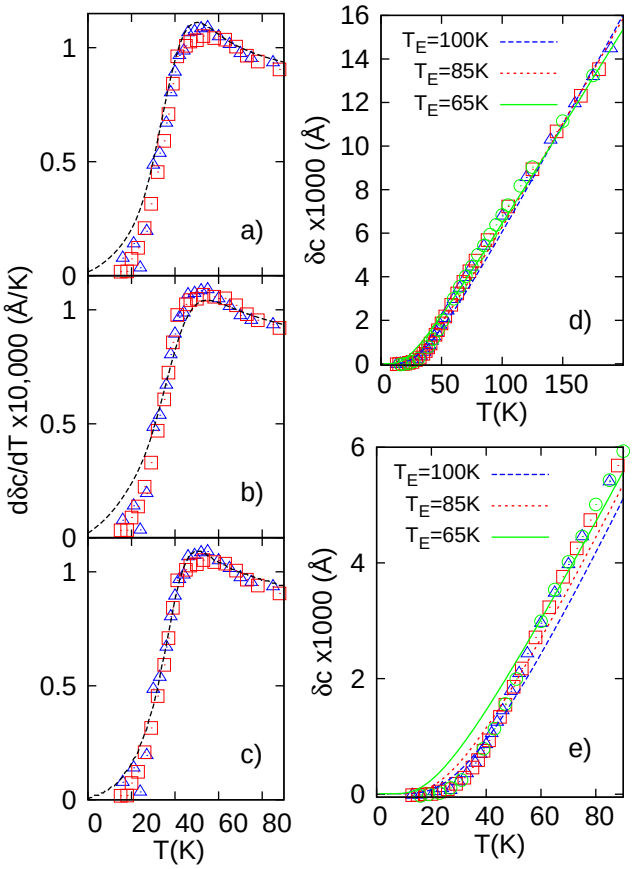

FIG. 5: Fits to the derivative data shown in the upper insert of Fig. 4 using a) a power law above and below T_o with a negative exponent, b) a power law above and below T_o with a postive exponent, and c) an exponential function below and a power law above T_o, as well as fits of the data shown in the main figure to an Einstein function in d) and e). The details of the fits are discussed in the main text.

$$\delta c = \frac{b}{\sqrt{2\pi}\sigma}\int_{-\infty}^{\infty} t^{1+\beta}\exp(-x^2/2\sigma^2)dx \qquad (2)$$

where

$$t = (T - T_o - x)/T_o \quad , \qquad (3)$$

and where $T_o = 35(2)$ K, $\sigma = 8.5(1.0)$ K, $b = 4.0(2) \times 10^{-4}$ Å for $T \geq T_o$ and $b = 0$ for $T \leq T_o$, and $\beta = -0.13(1)$. The Gaussian convolution roughly accounts for rounding of the power law behavior. The data and fit are shown in Fig. 4 for $0 < T < 80$ K. The lower insert of the main figure shows the same fit over a wider temperature range $0 < T < 200$ K. The upper inset shows $d(\delta c)/dT$ vs T for $H = 800$ Oe and the temperature derivative of the fit shown in the main figure. The bottom panel shows the fit minus the data multiplied by 10^4. The fits are excellent representations of the observed T dependence of c and, along with recent GGA calculations [4] suggest the model for the behavior discussed below.

To investigate whether using a power law or exponential temperature dependence below T_o would be consistent with the data, we tried several other fits to the same data and examples are shown in Fig. 5. For the comparison, we fit the temperature derivative of δc vs T using

$$\frac{d}{dT}(\delta c) = \frac{1}{\sqrt{2\pi}\sigma}\int_{-\infty}^{\infty}(at^{\beta} + d)\exp(-x^2/2\sigma^2)dx \qquad (4)$$

for $T > T_o$ and, for $T < T_o$,

$$\frac{d}{dT}(\delta c) = \frac{1}{\sqrt{2\pi}\sigma}\int_{-\infty}^{\infty}(a'(-t)^{\beta} + d')\exp(-x^2/2\sigma^2)dx \qquad (5)$$

with the results shown in Table II for the cases where $\beta < 0$ and $a' = 0$ (column A), $\beta < 0$ and $a' \neq 0$ (column B and panel a of Fig. 5), and $\beta > 0$, with $d = d'$ for continuity at T_o and $d' = -a'$ to ensure that $\frac{d}{dT}(\delta c) = 0$ at $T = 0$ (column C and panel b of Fig. 5). We also include (column D and panel c of Fig. 5) a fit where Eq. 5 was replaced for $T < T_o$ by,

$$\frac{d}{dT}(\delta c) = \frac{1}{\sqrt{2\pi}\sigma}\int_{-\infty}^{\infty} a'(\exp(-h/T)-1)\exp(-x^2/2\sigma^2)dx \qquad (6)$$

where, for continuity at T_o, we set $d = a'(\exp(-h/T_o) - 1)$. This is to explore whether an exponential function might work better for $T < T_o$. The results are shown in panel c. The fits shown in panels a, b and c were done over the temperature range $10 < T < 200$ K, but are shown, for clarity, over the smaller range $10 < T < 80$ K. Well above $T > 80$ K, the three fits are excellent and are indistinguishable. In each of these three fits, the rounding was set to be $\sigma = 8.5$ K, the value used in the fit shown in Fig. 4. No significant improvement was found by varying the amount of rounding and the rounding could not be reduced significantly without reducing the quality of the fit. The second and third columns of fitting results of Table II are similar, but with opposite signs for the exponent β. The significant rounding makes it difficult to distinguish between a positive and negative value for β; using a positive β yields a similar quality fit (panel a of Fig. 5 to that shown in Fig. 4. Panel a and b of Fig. 5, corresponding to the second and third column of fitting results in Table II, show that adding a low T power law results in a fit of poorer quality at low T. Panel c of Fig. 5, corresponding to the last column of fitting results in Table II, illustrates the inclusion of an exponential low T behavior. Although this yields better results than a low T power law behavior, the fit is clearly less good than the fits done with no function below T_o.

TABLE II: Fit parameters using Eq. 4, 5 and 6 with fixed $\sigma = 8.5$ K, as described in the text. The units are K for T_o and h and Å/K for a, a', d and d'.

	A	**B**	**C**	**D**
	Eq. 4	Eq. 4 & 5	Eq. 4 & 5	Eq. 4 & 6
T_o	35(2)	40(2)	41(2)	44(2)
β	-0.13(1)	-0.12(1)	0.26(1)	0.275(10)
$a(\times 10^5)$	9.86(30)	9.6(5)	-4.25(30)	-1.35(10)
$a'(\times 10^5)$	-	20(1)	-1.38(10)	0.45(3)
h	-	-	-	12.9(5)
d	0	0	$-a'$	$a'(e^{-h/T_o} - 1)$
d'	-	$-a'$	$-a'$	-

The large parameter $\sigma = 8.5(1.0)$ K in the Gaussian convolution is a physically meaningful parameter intrinsic to LCO. It cannot be a description of rounding caused by impurities, defects, surfaces, or interfaces because the fits are essentially the same for both single crystals, which vary significantly in quality, and the bulk powder.

It was previously shown, using neutron scattering results, [10] that an Einstein-like function [12] of the form

$$y(T) = y(0)[1 + \alpha(\coth(\frac{T_E}{2T}) - 1)] \quad (7)$$

is not as good a description of the data as the power law behaviors. We show such fits to the high resolution x-ray data for δc vs T in panels d and e of Fig. 5 with three different values of T_E. Over the large temperature range shown in panel d, the fits appear fairly good, but the same fits shown in panel e over the temperature range $10 < T < 90$ K demonstrate that, in the region near T_o, the fits are quite poor for any reasonable value of T_E.

Conclusions

We have demonstrated that the temperature dependence of the c lattice parameter in LCO single crystals for $T > T_o$ is well described by a power law behavior in the parameter $T - T_o$ and essentially no temperature change for $T < T_o$, when convoluted with a Gaussian function with a significant width of 8.5 K. This behavior is not altered by a field $H = 800$ Oe applied perpendicular to c. The behavior, including the amount of rounding, is nearly the same in two crystals that exhibit a different degree of crystallinity. Bulk LCO particles show the same behavior in the change of c with temperature, though the c parameter itself is slightly larger in the particles. We observed no significant difference upon cooling and heating in any of the samples. We conclude that, for large crystals and bulk powders, the transition at T = To is insensitive to small applied fields, differences in crystallinity, thermal cycling procedures or, with respect to the temperature dependence, the size of the system. On the other hand, previous experiments [6] using very small nanoparticles, where all spins are near particle surfaces, showed that as the core regions disappear, the transition near T_o does as well, [6] demonstrating that the transition is associated with the core regions far from interfaces.

The ferromagnetism in single crystals [13] and bulk powders [5] is very different, being much smaller in the single crystals and exhibiting a larger difference between zero-field cooling and cooling in a field. The dependence of the ferromagnetic moment on the abundance of surfaces and impurity interfaces, including twin boundaries, shows that ferromagnetism is associated [5, 6] with them and not the core regions. Hence, the transition in the core regions is unaffected by the ferromagnetic moment, which is why suppressing the ferromagnetism with the applied field has no discernible effect on the transition observed near T_o.

Recent results of GGA calculations [4] give clues to the possible origin of the transition near $T_o = 35$ K. First, the energy was found to be minimized for $\delta y \approx 0.052$. Second, at this value of δy, a magnetic state is approximately 3.2 meV/Co above a nonmagnetic state. Although the calculations indicate a ferromagnetic moment forming in the magnetic state, we note that an antiferromagnetic interaction dominates in the experiments, as indicated by the Curie-Weiss fits, and, in the core region, neither antiferromagnetic nor ferromagnetic long range ordering is observed for $T > 10$ K [5]. Magnetic correlations are observed for $\delta y < 0.052$ in the experiments. Finally, the magnetic state energy is decreased as δy decreases. We describe a model consistent with these results as well as those of the experiments.

At low temperature, the system is nonmagnetic and, because the value $\delta y \approx 0.052$ represents the minimum energy, it does not change with temperature. Previous inelastic neutron scattering experiments have been interpreted in terms of a thermally activated process; [8, 14] a fit of the inelastic neutron peak intensity vs T to an exponential thermal activation of the form $I \propto \exp(-E/k_BT)$ yields an activation temperature of 120 K. [8] The GGA calculations predict an activation temperature of approximately 37 K. We see from the fits of the data shown in Fig. 5 that an exponential fit tends to yield an activation temperature significantly higher than the T_o used in power law fits. As such, the higher characteristic temperature from the inelastic scattering fit is not necessarily inconsistent with the data and the power law fits obtained in this study or the GGA calculation results. The similarity of the inelastic scattering fits and the fits in panels d and e in Fig. 5 suggest that the inelastic scattering and structural phenomena are related. It is clear that the magnetic state is thermally activated, likely starting at local sites as T increases. As T continues to increase, more sites are thermally activated to the magnetic state and they become significant in number when T becomes comparable to the activation energy 3.2 meV/Co indicated by the calculations. [4] Note that 3.2 meV corre-

sponds to a temperature of 37 K, which is very close to the experimental value $T_o = 35$ K for the transition given by the power law fits shown in Fig. 4 and Table II. At $T = T_o$, the magnetic sites are dense enough to percolate, forming a long range cluster. A power law behavior in $T - T_o$ is typical of cluster percolation, [15] but the transition at the percolation threshold is clearly rounded.

The activated magnetic regions will tend to have a larger bond angle. [4] Because the experiments measure the average lattice parameters, two effects could lead to the observed rounding of the transition. First, the lattice strain caused by the formation of magnetic clusters is relatively long-ranged and the local lattice parameters associated with magnetic and nonmagnetic are not distinct values but rather vary with the proximity to the boundaries of the clusters. Second, the magnetic sites are not randomly excited, but rather, to reduce the strain energy, are more likely next to other magnetic sites. These two effects from the strain energy should result in a deviation from the power law behaviors characteristic of random site percolation [15] when T is close to T_o. The large value of the rounding reflects the large amount of lattice strain from the lattice mismatch of the nonmagnetic and magnetic regions.

We have shown that the temperature dependence of the lattice parameter c can be modeled by a nonmagnetic state at low T and an activated magnetic state with a percolation threshold for magnetic clusters near T_o. To better model the percolation of magnetic clusters in LCO, one would need to consider the competing energies and bond angles between the nonmagnetic and magnetic regions, the magnetic ordering energy, the lattice strain energies, and the dependence of the average lattice parameter c on the inhomogeneous bond angle distribution.

Use of the Stanford Synchrotron Radiation Lightsource, SLAC National Accelerator Laboratory, is supported by the U.S. Department of Energy, Office of Science, Office of Basic Energy Sciences under Contract No. DE-AC02-76SF00515. Work at Argonne National Laboratory (crystal growth and characterization) was supported by the U.S. Department of Energy, Office of Science, Basic Energy Sciences, Materials Science and Engineering Division.

[1] N. Sundaram, Y. Jiang, I. E. Anderson, D. P. Belanger, C. H. Booth, F. Bridges, J. F. Mitchell, T. Proffen, and H. Zheng, Phys. Rev. Lett. **102**, 026401 (2009).

[2] Y. Jiang, F. Bridges, N. Sundaram, D. P. Belanger, I. E. Anderson, J. F. Mitchell, and H. Zheng, Phys. Rev. B **80**, 144423 (2009).

[3] S. Medling, Y. Lee, H. Zheng, J. F. Mitchell, J. W. Freeland, B. N. Harmon, and F. Bridges, Phys. Rev. Lett. p. 157204 (2012).

[4] Y. Lee and B. N. Harmon, J. Appl. Phys. **113**, 17E145 (2013).

[5] A. M. Durand, T. J. Hamil, D. P. Belanger, S. Chi, F. Ye, J. A. Fernandez-Baca, Y. Abdollahian, and C. H. Booth, J. Phys.: Condens. Matter **27**, 126001 (2015).

[6] A. M. Durand, D. P. Belanger, T. J. Hamil, F.Ye, S. Chi, J. A. Fernandez-Baca, C. H. Booth, Y. Abdollahian, and M. Bhat, J. Phys.: Condens. Matter **27**, 176003 (2015).

[7] V. V. Mehta, N. Biskup, C. Jenkins, E. Arenholz, M. Varela, and Y. Suzuki, Phys. Rev. B **91**, 144418 (2015).

[8] A. Podlesnyak, S. Streule, J. Mesot, M. Medarde, E. Pomjakushina, K. Conder, A. Tanaka, M. W. Haverkort, and D. I. Khomskii, Phys. Rev. Lett. **97**, 247208 (2006).

[9] M. A. Korotin, S. Y. Ezhov, I. V. Solovyev, V. I. Anisimov, D. I. Khomskii, and G. A. Sawatzky, Phys. Rev. B **54**, 5309 (1996).

[10] A. M. Durand, D. P. Belanger, C. H. Booth, F. Ye, S. Chi, J. A. Fernandez-Baca, and M. Bhat, J. Phys.: Condens. Matter **25**, 382203 (2013).

[11] S. El-Khatib, D. Phelan, J. G. Barker, H. Zheng, J. F. Mitchell, and C. Leighton, Phys. Rev. B **92**, 060404 (2015).

[12] K. Asai, O. Yokokura, N. Nishimori, H. Chou, J. M. Tranquada, G. Shirane, S. Higuchi, Y. Okamima, and K. Kohn, Phys. Rev. B **50**, 3025 (1994).

[13] J.-Q. Yan, J.-S. Zhou, and J. B. Goodenough, Phys. Rev. B **69**, 134409 (2004).

[14] D. Phelan, D. Louca, S. Rosenkranz, S.-H. Lee, Y. Qiu, P. J. Chupas, R. Osborn, H. Zheng, J. F. Mitchell, J. R. D. Copley, et al., Phys. Rev. Lett. **96**, 027201 (2006).

[15] D. Stauffer and A. Aharony, Introduction to Percolation Theory (Taylor and Francis, Philadelphia, 1994).